Hypothalamic Macrophage Inducible Nitric Oxide Synthase Mediates Obesity-Associated Hypothalamic Inflammation

Chan Hee Lee[1,2], **Hyo Jin Kim**[2,4], **Yong-Soo Lee**[3], **Gil Myoung Kang**[2], **Hyo Sun Lim**[2,4], **Seung-hwan Lee**[4], **Do Kyeong Song**[5], **Obin Kwon**[5], **Injae Hwang**[6], **Myeongjoo Son**[7], **Kyunghee Byun**[7], **Young Hoon Sung**[2,3], **Seyun Kim**[8], **Jae Bum Kim**[6], **Eun Young Choi**[4], **Young-Bum Kim**[9], **Keetae Kim**[10], **Mi-Na Kweon**[3], **Jong-Woo Sohn**[1,8], and **Min-Seon Kim**[5,11,*]

[1]Biomedical Science and Engineering Interdisciplinary Program, Korea Advanced Institute of Science and Technology, Daejeon 34141, Korea

[2]Asan Institute for Life Sciences, University of Ulsan College of Medicine, Seoul 05505, Korea

[3]Department of Convergence Medicine, University of Ulsan College of Medicine, Seoul 05505, Korea

[4]Department of Biomedical Sciences, University of Ulsan College of Medicine, Seoul 05505, Korea

[5]Division of Endocrinology and Metabolism, Department of Internal Medicine, University of Ulsan College of Medicine, Seoul 05505, Korea

[6]National Creative Research Initiatives Center for Adipose Tissue Remodeling, School of Biological Sciences, Institute of Molecular Biology and Genetics, Seoul National University, Seoul 08826, Korea

[7]Department of Anatomy and Cell Biology, Gachon University College of Medicine, Incheon 21565, Korea

[8]Department of Biological Sciences, Korea Advanced Institute of Science and Technology, Daejeon 34141, Korea

[9]Division of Endocrinology, Diabetes and Metabolism, Department of Medicine, Beth Israel Deaconess Medical Center and Harvard Medical School, Boston, MA 02215, USA

[10]Department of New Biology, DGIST, Daegu 42988, Korea

[11]Lead Contact

*Correspondence: mskim@amc.seoul.kr.

SUMMARY

Obesity-associated metabolic alterations are closely linked to low-grade inflammation in peripheral organs, in which macrophages play a central role. Using genetic labeling of myeloid lineage cells, we show that hypothalamic macrophages normally reside in the perivascular area and circumventricular organ median eminence. Chronic consumption of a high-fat diet (HFD) induces expansion of the monocyte-derived macrophage pool in the hypothalamic arcuate nucleus (ARC), which is significantly attributed to enhanced proliferation of macrophages. Notably, inducible nitric oxide synthase (iNOS) is robustly activated in ARC macrophages of HFD-fed obese mice. Hypothalamic macrophage iNOS inhibition completely abrogates macrophage accumulation and activation, proinflammatory cytokine overproduction, reactive astrogliosis, blood-brain-barrier permeability, and lipid accumulation in the ARC of obese mice. Moreover, central iNOS inhibition improves obesity-induced alterations in systemic glucose metabolism without affecting adiposity. Our findings suggest a critical role for hypothalamic macrophage-expressed iNOS in hypothalamic inflammation and abnormal glucose metabolism in cases of overnutrition-induced obesity.

In Brief

Lee et al. demonstrate in mice that, upon prolonged high-fat diet feeding, hypothalamic macrophages proliferate, expand their pool, and sustain hypothalamic inflammation. Moreover, they show that hypothalamic macrophage iNOS inhibition diminishes macrophage activation, astrogliosis, blood-brain-barrier permeability, and impaired glucose metabolism in diet-induced obese mice.

Graphical Abstract
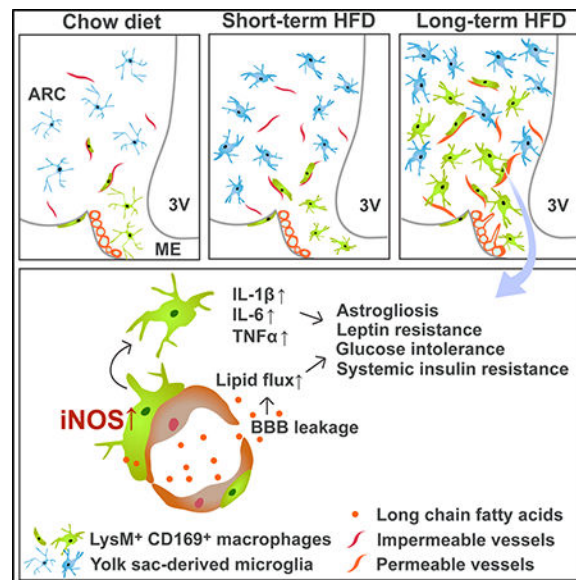
INTRODUCTION

Obesity has become a leading health concern in westernized countries, as obesity increases risks for type 2 diabetes, cardiovascular disease, Alzheimer's disease, sleep apnea, osteoarthritis, and certain types of cancers in obese patients (Rubenstein, 2005). Substantial evidence suggests that chronic inflammation in peripheral metabolic organs is a major contributor to the development of obesity-associated insulin resistance and metabolic derangement (Glass and Olefsky, 2012; Gregor and Hotamisligil, 2011). In the adipose tissue, macrophages are activated upon consumption of a high-fat diet (HFD). Once activated, they initiate inflammatory responses, which lead to insulin resistance in adipose tissue and eventually the development of type 2 diabetes (Lumeng and Saltiel, 2011).

The CNS controls body weight and glucose metabolism, primarily through the hypothalamus (Schwartz et al., 2000). The hypothalamic arcuate nucleus (ARC) is specifically crucial for maintaining energy balance and glucose homeostasis. ARC neurons detect blood-born metabolic signals, such as leptin, insulin, ghrelin, glucose, and fatty acids, to coordinate a series of adaptive responses (Schwartz et al., 2000). Similarly to HFD-induced adipose tissue inflammation, chronic HFD intake induces low-grade inflammation in the rodent hypothalamus, which is characterized by increased expression of proinflammatory cytokines, including interleukin (IL)-1β, IL-6, and tumor necrosis factor-a (TNF-α) (De Souza et al., 2005). Animals on a chronic HFD also display hypothalamic activation of multiple inflammatory signaling pathways, including those involving the toll-like receptor 4 (TLR4), myeloid differentiation factor 88 (Myd-88), c-Jun N-terminal kinase (JNK), and IκB kinase-β-nuclear factor-κB (IKKβ-NFκB) (Cai and Liu, 2011). Furthermore, studies indicate that activation of those inflammatory signaling cascades mediates overnutrition-related impairment of leptin and insulin signaling in hypothalamic neurons (Cai and Liu, 2011). Thus, hypothalamic inflammation plays a key role in the development of diet-induced obesity (DIO) and subsequent metabolic complications.

Although evidence clearly shows that an HFD induces hypothalamic inflammation, it is largely unknown how neurons, glial cells, and immune cells interact during inflammation as well as the molecular mediators controlling these processes. Microglia are important innate immune cells in the CNS that sense pathogenic invasion or tissue damage (Perry et al., 2010). Microglia have been considered to be CNS macrophages (Gordon and Taylor, 2005); however, a recent study investigating gene expression patterns of microglia and peritoneal macrophages suggests that CNS-resident microglia have a distinct origin from peripheral macrophages (Gosselin et al., 2014). Most microglia arise from primitive hematopoietic cells in the yolk sac (Ginhoux et al., 2010). They populate the neuroepithelium during the early embryonic period and maintain their population through lifelong self-renewal. In contrast to yolk-sac-derived microglia (Ginhoux et al., 2010; Schulz et al., 2012), a significant proportion of peripheral organ macrophages develop from circulating monocytes that originate from fetal liver during the late embryonic period and from bone marrow in the postnatal stage (Ginhoux and Jung, 2014).

Microglia in the hypothalamic ARC are readily activated following short-term exposure to an HFD or saturated fatty acids (Thaler et al., 2012; Valdearcos et al., 2014). Activated

microglia are thought to be key players in hypothalamic inflammation because they release proinflammatory cytokines and chemokines (Smith et al., 2012). A recent study showed that monocyte-derived macrophages are also present in the hypothalamus, especially the median eminence (ME) and ARC (Gao et al., 2014; Kälin et al., 2015). However, a role for macrophages in hypothalamic inflammation has not been studied. Another study demonstrated enhanced migration of circulating immune cells to the hypothalamus in HFD-fed obese mice (Buckman et al., 2014). In that study, the mice received irradiation of the whole body, including the head, before bone marrow transplantation. Those findings should be interpreted with caution, as head irradiation can disrupt the integrity of the blood-brain barrier (BBB) and allow the artificial invasion of bone-marrow-derived cells into the brain (Mildner et al., 2011). Indeed, there have been numerous debates on whether bone-marrow-derived monocytes and macrophages contribute to CNS inflammation in adulthood (Ajami et al., 2007; Hickey and Kimura, 1988; Prinz et al., 2011). Given this uncertainty, the issue of which immune cells are involved in HFD-induced hypothalamic inflammation should be precisely investigated.

In this study, we show that activation and expansion of hypothalamic macrophages contribute to hypothalamic inflammation in mice chronically exposed to fat-rich diets. Furthermore, our findings suggest that inducible nitric oxide synthase (iNOS) activation in hypothalamic macrophages links chronic HFD consumption to hypothalamic inflammation by increasing vascular permeability and lipid influx into the hypothalamic ARC.

RESULTS

Macrophage Pool Expansion in the ARC of DIO Mice

To investigate the role of macrophages in HFD-induced hypothalamic inflammation, we generated mice that express GFP in lysozyme M (LysM)-expressing myeloid cells (LysM^{GFP} mice). When young male LysM^{GFP} mice were fed a standard chow diet (CD), GFP$^+$ myeloid cells were frequently observed in the ME and along the leptomeningeal lining (Figure 1A). Linear GFP$^+$ cells were often identified in the hypothalamic parenchyma, and ramified microglia-like GFP$^+$ cells were found at the ARC and ME border (Figure 1A).

Notably, a significant expansion of GFP$^+$ myeloid pool was found in the hypothalamic ARC of obese mice placed on a HFD (58% fat) for 4 and 20 weeks (Figure 1A). This expansion was most prominent in the mediobasal and caudal regions of the ARC (Figure S1A), but not in other hypothalamic areas (Figure S1B). Additionally, the morphology of the ARC GFP$^+$ cells changed from linear to ramifying microglia-like (Figures 1A and S1A). The number and morphology of ME macrophages changed as well. The time course study revealed that ARC GFP$^+$ cells expanded significantly after 2 weeks on an HFD (Figure 1B).

To identify the spatial relation between GFP$^+$ cells and hypothalamic vasculature, we performed dual staining of GFP and the vascular marker platelet and endothelial cell adhesion molecule 1 (PECAM1). In CD-fed lean mice, rod-shaped GFP$^+$ cells were mostly adjacent to the hypothalamic microvasculature (Figure 1C). GFP$^+$ cells were located between PECAM1$^+$ blood vessels and glial fibrillary acidic protein (GFAP)$^+$ astrocyte processes (Figure S1C), indicating that these cells may be perivascular macrophages

(PVMs). After 7 days of HFD exposure, linear GFP$^+$ cells enlarged and elongated, but they were still associated with blood vessels (Figure 1C). At 4 weeks of HFD exposure, they enlarged further, and more than a half of GFP$^+$ cells were located in the ARC parenchyma proximal to microvessels. In 20-week HFD-fed mice, the numbers of perivascular and parenchymal GFP$^+$ cells increased profoundly and exhibited marked morphological changes, suggesting a highly activated state (Figure 1D). In addition, blood vessel length and diameter increased substantially (Figure 1D), which could be an indicator of HFD-induced hypothalamic angiopathy (Yi et al., 2012).

To verify whether both perivascular and parenchymal GFP$^+$ cells are monocyte-derived macrophages, we performed double immunostaining of GFP and CD169, a marker of monocyte-derived macrophages (Figure 1E). More than 90% among LysM^{GFP} cells coexpressed CD169 in both CD- and 20 week-HFD-fed condition (CD: 97.1% ± 0.8%; HFD: 94.5% ± 0.7%). Conversely, most CD169$^+$ cells coexpressed GFP (CD: 94.1% ± 0.8%; HFD: 95.7% ± 1.0%). Linear LysM^{GFP} cells robustly expressedCD169(Figure1E,i). Likewise, amoeboid highly activated microglia-like LysM^{GFP} cells manifested strong immunoreactivity to CD169 in the cell body and processes (Figure 1E, ii). Of note, most ramified microglia-like LysM^{GFP} cells also expressed CD169 in the body, albeit weakly (Figure 1E, iii). In CD-fed lean mice, a major proportion of ARC CD169$^+$ LysM$^+$ cells were linear shaped (Figures 1E and1F). Upon prolonged HFD feeding, linear, amoeboid, and ramified forms of CD169$^+$ LysM$^+$ cells were accumulated in the ARC (Figures 1E and 1F). These findings raised the possibility that most LysM^{GFP} cells may be derived from monocytes or macrophages, regardless of their shapes. However, it is also possible that yolk-sac-derived microglia may induce the expression of LysM and/or CD169 in response to chronic HFD. On the other hand, LysM expression was found in some population of neurons across the many brain regions (Orthgiess et al., 2016). Dual staining of GFP with the neuronal marker microtubule-associated protein 2 (MAP2) in LysM^{GFP} mice revealed that none of the ARC neurons expressed LysM (Figure S1D).

A recent study revealed enhanced recruitment of peripheral myeloid cells into the ARC during an HFD feeding (Valdearcos et al., 2017). In that study, accumulation of myeloid cells without markers of resident microglia or blood-born cells was also observed in the ARC of mice on an HFD for 4 weeks. We therefore tested the possibility of *in situ* proliferation of hypothalamic macrophages. Mice with tdTomato expression in LysM cells (LysM^{tdT} mice) were fed HFD for the indicated periods and intraperitoneally injected with 5-bromodeoxyuridine (BrdU) for 5 days before sacrifice. The numbers of LysM^{tdT} cells with BrdU immunoreactivity started to increase from 1 week HFD consumption (Figure 1G). Ki67/GFP dual staining in DIO mice fed HFD for 20 weeks also revealed increased Ki67-expressing GFP$^+$ cells in the ARC and along the meningeal lining (Figure S1E). In agreement with these data, we found an increased number of BrdU$^+$ CD169$^+$ proliferating macrophages in the ARC of DIO mice (Figure S1F). Our findings suggested that *in situ* self-renewal of LysM$^+$ or CD169$^+$ myeloid cells contributes to hypothalamic macrophage accumulation under DIO condition. Alternatively, monocytes could become Ki67 or BrdU positive prior to their entry from the bloodstream into the hypothalamus.

HFD Induces Hypothalamic Macrophage Expansion and Activation via iNOS-Dependent Mechanism

To probe for critical molecules involved in HFD-induced hypothalamic macrophage activation and expansion, we screened the mediobasal hypothalamus (MBH) of 20-week HFD-fed mice for expression changes in genes implicated in obesity-related inflammation and vascular remodeling. Using qPCR analysis, we observed remarkable increases in the mRNA expression levels of *iNos*, hypoxia-inducible factor-1α (*Hif-1α*), and proinflammatory cytokines *Il-1β*, *Il-6*, and *Tnfa* in the MBH of HFD-fed obese mice compared with those of CD-fed lean controls. In contrast, vascular endothelial growth factor-A (*Vegfa*) and endothelial NOS (*eNos*) mRNA expression levels were lower in DIO mice (Figure S2A).

Dual staining of iNOS and GFP in the ARC of LysM^{GFP} mice revealed rod-shaped GFP$^+$ cells with potent immunoreactivity against iNOS (Figure 2A). Similarly, we detected high iNOS expression in ARC CD169$^+$ macrophages (Figure 2B). Iba1 and iNOS double immunostaining also showed strong iNOS staining in cross-sectioned thick PVM-like myeloid cells and weak staining in ramified parenchymal microglia (Figure S2B). In contrast, GFAP$^+$ astrocytes and MAP2$^+$ neurons had no iNOS immunoreactivity (Figure S2C). A time course study revealed that ARC iNOS expression, especially in the CD169$^+$ macrophages, increased from 1 week after HFD feeding (Figure 2C).

To investigate iNOS regulation of hypothalamic macrophages, the NO donor, sodium nitroprusside (1 μg) was injected daily into the lateral cerebroventricle of CD-fed LysM^{GFP} mice for 5 days. Changes in hypothalamic macrophages were examined using GFP staining. Similarly to HFD-fed mice, the number of GFP$^+$ cells in the ARC increased after 5 days sodium nitroprusside administration in lean animals (Figure 2D). BrdU study, in which BrdU was injected daily during the 5-day sodium nitroprusside treatment, showed increased numbers of BrdU$^+$ CD169$^+$ proliferating macrophages in the ARC after sodium nitroprusside treatment (Figure 2E). MBH proinflammatory cytokine expression showed a tendency of increase after sodium nitroprusside treatment (Figure 2F). Therefore, NO overproduction by ARC macrophages in the HFD-fed condition may stimulate *in situ* proliferation and activation of ARC macrophages in the early course of DIO.

Central iNOS Inhibition Ameliorates Hypothalamic Macrophage Activation and Improves Glucose Metabolism in DIO Mice

Next, we studied whether hypothalamic iNOS inhibition can prevent hypothalamic macrophage activation in DIO mice. We administered the non-specific NOS inhibitor L-N^G-nitroarginine methyl ester (L-NAME) (0.1 mg) or the iNOS inhibitor L-N6-(1-iminoethyl)lysine (L-NIL) (0.1 mg) intracerebroventricularly (ICV) for 5 days in 20-week HFD-fed LysM^{GFP} mice. The dose of NOS inhibitors were selected because this dose did not affect food intake or body weight (Figures S3A and S3B). DIO-induced expansion of GFP$^+$ cells in the ARC significantly reduced following ICV treatment with L-NAME or L-NIL for 5 days (Figures 3A and 3B). Treatment with inactive enantiomer D-NAME (0.1 μg for 5 days) did not reverse HFD-induced changes in ARC GFP$^+$ cells (Figure S3C), indicating that the effect of L-NAME treatment on GFP$^+$ cells was NOS specific. In

addition, elevated hypothalamic Il-1β and Il-6 levels in 20-week HFD-fed mice were normalized following the short-term L-NIL treatment (Figure 3C). Obese mice on an HFD for 20 weeks had impaired ICV leptin-induced anorexia and hypothalamic STAT3 phosphorylation; however, this impairment was significantly improved following a 5-day treatment of L-NAME or L-NIL (Figures 3D–3F). These data suggest a crucial role for iNOS in HFD-induced hypothalamic macrophage activation, inflammation, and leptin resistance. Despite improved hypothalamic responses to exogenous leptin, body weight changes during the treatment period did not differ between treatment and control groups (data not shown). Thus, the observed beneficial effects of central iNOS inhibition were unrelated to weight loss.

We also studied the effect of chronic CNS iNOS inhibition on hypothalamic macrophages. Twenty-week HFD-fed mice were infused with L-NIL over a 4-week period using an osmotic pump (1.2 ng/hr) connected through the lateral cerebroventricle. Chronic L-NIL treatment returned the elevated NO to normal levels in the hypothalamus of DIO mice without affecting plasma NO levels (Figure S4A). These data suggest that this treatment may not alter systemic NOS activity. Similar to short-term L-NIL treatment, 4-week L-NIL infusion completely blocked the expansion and activation of ARC GFP$^+$ cells (Figure 3G). Therefore, chronic inhibition of brain iNOS activity during HFD feeding can reverse or prevent the expansion and activation of hypothalamic macrophages.

Long-term central treatment with iNOS inhibitor did not alter food intake, body weight, and fat mass (Figure S4B). A previous study showed that activated iNOS induces insulin resistance in skeletal muscle and glucose intolerance (Perreault and Marette, 2001). Thus, we examined glucose metabolism in L-NIL-treated DIO mice. Chronic L-NIL treatment in DIO mice significantly decreased plasma glucose levels during glucose, insulin, and pyruvate tolerance tests (Figure 3H). The homeostatic model assessment for insulin resistance (HOMA-IR) index, a casual marker of peripheral insulin sensitivity, tended to decrease in L-NIL-treated mice, although fasting blood glucose and triglyceride concentrations were not significantly altered (Figure S4C). Pancreatic euglycemic clamp study revealed that reduced glucose infusion rate (GIR) in DIO mice was normalized by chronic L-NIL treatment (Figure 3I), suggesting improved insulin resistance. Insulin-promoted glucose disappearance rate (Rd) and insulin-suppressed hepatic glucose production (HGP) during the clamp period were both blunted in DIO mice (Figures 3I and S4D). L-NIL treatment in obese mice reversed the decreased Rd without significant effect on HGP (Figures 3I and S4D). These results demonstrate that central iNOS inhibition improves systemic glucose clearance.

To further understand the mechanism by which central L-NIL treatment improved systemic glucose metabolism, we measured the expression of hypothalamic suppressor of cytokine signaling 3 (_Socs3_) and protein tyrosine phosphatase 1B (_Ptp1b_). These proteins are known to be negative regulators of hypothalamic leptin and insulin signaling, and their expression increases in HFD-fed obese animals (Pedroso et al., 2014; Picardi et al., 2008). Hypothalamic _Socs3_ and _Ptp1b_ expression was increased in DIO mice and normalized with chronic treatment of iNOS inhibitor (Figure 3J), suggesting that SOCS3 and PTP1B may mediate the metabolic effects of central iNOS blockade. It has been recently shown that the

hypothalamus regulates adipose tissue immune function (Kim et al., 2015). Therefore, we examined the effect of CNS iNOS inhibition on the peripheral immune system. Plasma TNF-α concentrations remained unchanged with chronic L-NIL treatment (Figure S4E). The numbers of leukocytes, macrophages, and T and B lymphocytes in the abdominal white adipose tissue was also unaltered in mice chronically administered ICV iNOS inhibitor (Figure S4F). Therefore, the metabolic improvements observed with CNS L-NIL treatment may not be mediated through systemic anti-inflammatory effects.

Macrophage iNOS Inhibition Mitigates HFD-Induced Hypothalamic Macrophage Activation and Altered Glucose Metabolism

To clarify the specific role of macrophage-expressed iNOS in HFD-induced hypothalamic inflammation and metabolic impairment, we generated the adeno-associated virus, which expresses both yellow fluorescent protein (YFP) and iNOS-targeting small hairpin RNA (LysM ^{iNOS}-AAV) in a Cre-dependent manner (Figure 4A). Before initiating the animal study, we tested the activity of LysM ^{iNOS}-AAV in Cre-recombinase-expressing RAW264.7 cells (Figure 4B). We then injected LysM ^{iNOS}-AAV into the bilateral ARC of LysM-Cre mice on a HFD for 15 weeks. Successful virus injection was confirmed by YFP expression in ARC LysM$^+$ cells (Figure 4C). There was no YFP expression in non-LysM$^+$ cells, confirming Cre-dependent AAV transfection. Dual iNOS and tdT staining revealed reduced iNos expression in LysM^{tdT} cells in mice injected with LysM ^{iNOS}-AAV (Figure 4D), indicating successful iNos knockdown in ARC LysM$^+$ cells. Bilateral intra-ARC injection of LysM ^{iNOS}-AAV potently reverted HFD-induced expansion of GFP$^+$ cell pool (Figure 4E). Similarly, LysM ^{iNOS}-AAV injection decreased hypothalamic proinflammatory cytokine expression and improved systemic glucose metabolism as well (Figures 4F and 4G). These data suggest a critical role of macrophage iNOS activation in diet-induced hypothalamic inflammation and subsequent systemic metabolic complications.

We finally tested adverse effect of iNOS inhibition on the phagocytic activity of microglia and macrophages. Notably, L-NIL treatment did not impair the phagocytic activity of BV2 microglia and RAW264.7 macrophage cells, whereas palmitate treatment reduced it (Figure S5A). Repeated ICV injection of L-NIL did not reduce the phagocytic ability of hypothalamic Iba1$^+$ cells as well (Figure S5B), suggesting that iNOS inhibition may not dampen hypothalamic microglia and macrophage-mediated phagocytosis.

iNOS Mediates HFD-Induced BBB Disruption, Lipid Accumulation, and Astrogliosis in the Hypothalamus

We examined whether iNOS activation contributes to other HFD-induced hypothalamic changes. In CD-fed lean mice, 5-day ICV administration of sodium nitroprusside strongly induced extravascular leakage of boron-dipyrromethene (BODIPY)-fatty acid in the ME and ARC (Figure 5A). In line with this, enhanced leakage of fluorescent-conjugated albumin was observed in the ARC of HFD-fed mice, which was reversed by chronic L-NIL treatment (Figure 5B). These results suggest that iNOS-induced NO overproduction in hypothalamic macrophages may increase vascular permeability and fatty acid flux in the ARC. Then, we examined hypothalamic lipid accumulation resulting from enhanced hypothalamic lipid flux in DIO animals. Lipid visualization using BODIPY 493/503 revealed significant lipid

accumulation in the hypothalamic interstitial space and macrophages of 5-week HFD-fed LysM[tdT] mice and in Iba1^{+} reactive microglia in the ARCof 20-weekHFD-fed mice (Figures 5C and 5D). These results indicate that hypothalamic macrophages and microglia could uptake lipids for clearance. Strikingly, chronic CNS iNOS inhibition robustly inhibited hypothalamic lipid accumulation in mice with prolonged HFD consumption (Figure 5D). These data confirm that iNOS plays an indispensable role in hypothalamic lipid over-load in cases of chronic fat-rich diet consumption. In addition, chronic L-NIL treatment significantly reduced the HFD-induced increase in vascular density in the ARC of obese mice (Figure 5E), implying a significant contribution of iNOS in HFD-induced hypothalamic vascular changes.

Astrocytes are important glial cells that support neuronal function and BBB integrity (Abbott et al., 2006). Reactive astrogliosis (i.e., reactive astrocyte hypertrophy and hyperplasia) is a common feature of neuroinflammation. This feature has been observed previously in the hypothalamus of mice with diet- or genetically induced obesity (Buckmanetal.,2013; Horvath et al.,2010; Thaler et al., 2012); however, the precise mechanisms mediating this phenomenon are not well understood. Consistent with the previous reports, we found significant astrogliosis in the ARC of DIO mice (Figure 5F). Notably, 4-week L-NIL treatment completely inhibited HFD-induced astrogliosis. By contrast,5-day ICV injection of sodium nitroprusside in lean mice did not induce hypothalamic astrogliosis (Figure 5F). These data suggest that hypothalamic iNOS activation may indirectly induce astrogliosis, possibly through increased lipid flux and hypothalamic inflammation. Similarly to L-NIL treatment, intra-ARC injection of LysM [iNOS]-AAV significantly diminished HFD-induced vascular changes and astrogliosis (Figures 5G and 5H). Overall, our results underscore that iNOS activation in LysM^{+} myeloid cells contributes significantly to the multi-faceted pathological processes of overnutrition-induced hypothalamic inflammation.

DISCUSSION

Activation and Expansion of Hypothalamic LysM^{+} CD169^{+} Macrophages upon HFD Feeding

This study characterizes LysM^{+} myeloid cells in the mouse hypothalamus in both resting and reactive states. More than 90% of them coexpress monocyte-derived macrophage marker CD169, supporting the notion that they may be hypothalamic macrophages. There is a concern about the use of LysM for tracing brain myeloid cells because some neuronal populations have been shown to express LysM (Orthgiess et al., 2016). We found that ARC LysM^{+} cells did not express neuronal marker MAP2 and showed the morphology distinct from neurons. Therefore, LysM can be used to trace macrophages in the ARC.

In the CD-fed condition, hypothalamic macrophages are rod shaped and closely apposing microvessels, implying that they may be PVMs. PVMs are localized to the interface between the CNS and vascular system. They express multiple receptors involved in pathogen-associated molecular pattern recognition, phagocytosis, cytokine responsiveness, antigen presentation, and co-stimulation (Serrats et al., 2010; Williams et al., 2001). Thus, PVMs could primarily coordinate innate and adaptive immune responses to immune or infectious

signals within the CNS. Another important role of PVMs could be to sense metabolic signals from circulation and control BBB functions. For example, PVMs secrete VEGF in response to an HFD-induced reduction in brain glucose uptake and maintain brain glucose uptake by increasing BBB glucose transporter 1 (GLUT1) expression (Jais et al., 2016).

A previous report showed that the resident microglia pool significantly expanded after 3 days of HFD feeding (Thaler et al., 2012), which supports the hypothesis that resident microglia are the first responders to hypothalamic fat overload. By contrast, we found that the LysM[+] myeloid pool did not expand significantly until 2 weeks after starting the HFD. Interestingly, LysM[GFP] cells were found in the ARC parenchyma following prolonged exposure to an HFD. They presented a ramified or reactive microglia-like morphology. Parenchymal LysM[GFP] cells were almost indistinguishable from reactive resident microglia based on morphological examination. Their proximity to the vasculature under HFD conditions suggests that PVMs may infiltrate into the ARC parenchyma and become microglia (parenchymal myeloid cells). Supporting this notion, microglia-shaped parenchymal LysM[GFP] cells did express macrophage marker CD169 in the body. These data may raise the possibility that linear-shaped LysM^{+} CD169^{+} cells can undergo a phenotypic switch to microglia-like cells when they migrate from the perivascular space to the ARC parenchyma. Alternatively, resident microglia might have inducible expression of LysM and CD169 upon activation by persistent exposure to HFD. A fate-mapping study is critically needed to confirm the ontogeny of parenchymal LysM^{+} cells.

Questions remain regarding the physiological roles and pathophysiological impacts of HFD-induced hypothalamic macrophage activation. Both hypothalamic resident microglia and macrophages have phagocytic activity (Serrats et al., 2010) and had intracellular lipid droplets in HFD-fed condition. Thus, resident microglia could prevent excessive lipid accumulation in the hypothalamic extracellular space, which is detrimental to neurons and other cellular populations, by clearing these lipids. If microglia-mediated lipid clearance was insufficient to prevent lipid accumulation, LysM[+] macrophages with higher phagocytic activity could potentially be recruited to the ARC parenchyma. These two cellular populations could release proinflammatory cytokines and chemokines and trigger the hypothalamic innate immune response to fatty acids. This response may be beneficial to maintain hypothalamic homeostasis initially but could become detrimental when it acts chronically.

Mechanism of HFD-Induced Expansion of Hypothalamic Macrophage Pool

There have been numerous debates on the contribution of peripheral immune cells to CNS inflammation in Alzheimer's diseases, Parkinson's diseases, multiple sclerosis, amyotrophic lateral sclerosis, and stroke (Prinz et al., 2011). Results from the bone marrow transplant experiment revealed enhanced recruitment of peripheral myeloid cells to the ARC after HFD feeding (Valdearcos et al., 2017). These observations point to a significant contribution of peripheral myeloid cells to the ARC myeloid pool expansion during the development of DIO.

Another line of evidence indicates that local proliferation of tissue macrophages is also an important mechanism for maintaining their pool. For instance, adipose-tissue macrophages

locally undergo cell division and maintain their pool by *in situ* proliferation under the conditions of monocyte depletion (Amano et al., 2014). Moreover, PVMs in the brain maintain a stable cellular pool without substantial exchange with blood cells for 46 weeks (Goldmann et al., 2016).

Time course BrdU study documented the presence of proliferating linear LysM^{+} or CD169^{+} myeloid cells in the ARC of mice on a HFD, and these changes were evident from the early course of HFD feeding. Furthermore, proliferating LysM^{+} CD169^{+} macrophages were observed in the ARC and leptomeningeal lining of obese mice fed a HFD for 20 weeks. These findings may indicate that, upon HFD feeding, hypothalamic LysM^{+} CD169^{+} macrophages expand their pool through self-renewal, which is similar to resident microglia (Ajami et al., 2007). However, we could not exclude the possibility that circulating LysM^{+} CD169^{+} myeloid precursors gain these proliferating markers before they enter the hypothalamus. Although it is unclear where the initiation of myeloid cell proliferation takes place, proliferating LysM^{+} CD169^{+} myeloid cells contribute to hypothalamic myeloid cell accumulation induced by chronic exposure to a fat-rich diet.

A Crucial Role for Macrophage iNOS in HFD-Induced Hypothalamic Inflammation

A previous study showed increased iNOS expression in skeletal muscle and fat tissue of mouse models of genetic and dietary obesity (Perreault and Marette, 2001). We consistently found enhanced iNOS expression in the hypothalamus of DIO mice. HFD-induced iNOS expression was prominent in linear-shaped LysM^{+} CD169^{+} macrophages. Moreover, central administration of an NO donor caused ARC macrophage expansion under CD-fed conditions, whereas blockage of CNS iNOS activity specifically in the ARC macrophages potently blocked ARC macrophage expansion and hypothalamic inflammation in DIO mice. These findings imply that hypothalamic macrophage-derived NO induces macrophage accumulation and activation. This mechanism may be important for sustaining hypothalamic inflammation in cases of chronic fat-rich diet consumption.

ARC iNOS activation may lead to increased lipid flux into the hypothalamus by increasing vascular permeability. ICV injection of sodium nitroprusside markedly increased the hypothalamic uptake of fluorescent fatty acids administered into systemic circulation. Furthermore, 4 weeks of treatment with an iNOS inhibitor completely rescued extravascular albumin leakage in DIO animals. These findings suggest that a centrally acting iNOS inhibitor could potentially be used to combat human disorders associated with disrupted BBB integrity.

Consistent with previous studies (Horvath et al., 2010; Thaler et al., 2012), we observed reactive astrogliosis in the hypothalamus of DIO mice and its reversal when injected with L-NIL and LysM [iNOS]-AAV. Because sodium nitroprusside administration in lean mice did not induce astrogliosis, iNOS is not likely to have a direct regulatory role in hypothalamic astrocyte pool. In addition, the increased vascular density in DIO mice, which was suggested to be hypothalamic angiopathy (Thaler et al., 2012), was significantly reduced by central iNOS inhibition. These results highlight the critical contribution of hypothalamic macrophage iNOS to HFD-induced hypothalamic astrogliosis and vascular remodeling.

Metabolic Implications of iNOS-Mediated Hypothalamic Inflammation in DIO Mice

In this study, hypothalamic iNOS inhibition significantly improved glucose intolerance and systemic insulin resistance along with enhanced glucose disposal in DIO mice. These findings are in line with metabolic phenotypes of *iNos*-encoding *Nos2* whole-body knockout mice (Perreault and Marette, 2001). The *Nos2*$^{-/-}$ mice developed obesity on an HFD but exhibited improved glucose tolerance, normal insulin sensitivity, and normal insulinstimulated glucose uptake in skeletal muscles. Therefore, HFD-induced iNOS activation in the hypothalamus and skeletal muscle contributes to the development of insulin resistance and abnormal glucose metabolism in DIO animals. In addition, inhibition of hypothalamic iNOS activity restored impaired hypothalamic STAT3 activation and acute anorexic response following exogenous leptin administration in DIO mice. Despite improved hypothalamic leptin signaling, food intake and body weight were unaltered by chronic central iNOS inhibition. Similarly to our findings, a recent paper has shown that tamoxifen-inducible dynein-related protein (DRP1) deletion in proopiomelanocortin (POMC) neurons improves glucose tolerance but does not alter body weight despite high leptin sensitivity (Santoro et al., 2017). In contrast to our findings, depletion of microglia and inhibition of IKKβ-NFκB signaling in CX3CR1^{+} microglia suppress food intake and weight gain during a HFD (Valdearcos et al., 2017). Our data on glucose homeostasis suggest microglia and CNS macrophages can impact blood glucose control by the brain in a manner that is independent of their role in regulating the hypothalamic control of body weight. It supports that microglia and macrophages have multiple functional roles in metabolic regulation and that iNOS may be involved in their role in glucoregulation.

Centrally administered iNOS inhibitor did not alter plasma NO and TNF-α levels or adipose tissue immune cell populations, indicating that brain iNOS does not play a regulatory role in systemic inflammation. Chronic low-grade hypothalamic inflammation was shown previously to disrupt peripheral insulin signaling and glucose homeostasis (Arruda et al., 2011). Consistently, in our study, inhibition of hypothalamic inflammation improved insulin resistance and glucose intolerance in mice on a prolonged HFD. The beneficial metabolic effects of central iNOS inhibition may be partly explained by improved leptin sensitivity and reduced hypothalamic *Socs3* and *Ptp1b* expression. Interestingly, a recent study showed that, in the hypothalamus, increased NO levels disrupt the insulin signaling through S-nitrosation of insulin receptor and Akt (Katashima et al., 2017). Future studies are needed to fully understand neural mechanisms or circuits mediating the effects of central iNOS blockade on peripheral glucose metabolism.

fMRI studies have demonstrated the association of MBH inflammation and gliosis to human obesity (Kreutzer et al., 2017; Thaler et al., 2012). Our experimental evidence in mice suggests a critical role for hypothalamic macrophages and their inducible NO overproduction in sustaining hypothalamic inflammation and inducing systemic metabolic complications in DIO. Therefore, our findings support targeting hypothalamic macrophage iNOS as part of therapeutic interventions for obesity-related metabolic disorders.

STAR★METHODS

KEY RESOURCES TABLE

REAGENT or RESOURCE	SOURCE	IDENTIFIER
Antibodies		
Rat monoclonal anti-BrdU	Novus	Cat# NB500–169; RRID: AB_10002608
Rat monoclonal anti-CD169	Biorad	Cat# MCA884; RRID: AB_322416
Rabbit polyclonal anti-GFAP	Millipore	Cat# AB5804; RRID: AB_2109645
Chicken polyclonal anti-GFP	Aves Labs	Cat# GFP-1010; RRID: AB_2313520
Goat polyclonal anti-Iba1	Abcam	Cat# Ab5076; RRID: AB_2224402
Mouse monoclonal anti-iNOS	BD Biosciences	Cat# 610328; RRID: AB_397718
Rabbit polyclonal anti-Ki67	Abcam	Cat# Ab66155; RRID: AB_1140752
Chicken polyclonal anti-MAP2	Abcam	Cat# Ab5392; RRID: AB_2138153
Rat monoclonal anti-PECAM1	BD Biosciences	Cat# 550274; RRID: AB_393571
Rabbit polyclonal anti-P-STAT3	Cell Signaling	Cat# 9131; RRID: AB_331586
Goat polyclonal anti-chicken, Alexa-Flour 488-conjugated	Invitrogen	Cat# A11039; RRID: AB_142924
Donkey polyclonal anti-goat, Alexa-Flour 488-conjugated	Invitrogen	Cat# A11055; RRID: AB_142672
Goat polyclonal anti-mouse, Alexa-Flour 647-conjugated	Invitrogen	Cat# A21236; RRID: AB_141725
Donkey polyclonal anti-rabbit, Alexa-Flour 488-conjugated	Invitrogen	Cat# A21206; RRID: AB_141708
Goat polyclonal, anti-rabbit, Alexa-Flour 633-conjugated	Invitrogen	Cat# A21070; RRID: AB_2535731
Goat polyclonal anti-rat, Alexa-Flour 488-conjugated	Invitrogen	Cat# A11006; RRID: AB_141373
Goat polyclonal anti-rat, Alexa-Flour 633-conjugated	Invitrogen	Cat# A21094; RRID: AB_141553
Rat monoclonal anti-B220, PerCP-conjugated	BD Biosciences	Cat# 553093; RRID: AB_394622
Rat monoclonal anti-CD11b, APC-Cy7-conjugated	BD Biosciences	Cat# 557657; RRID: AB_396772
Hamster monoclonal anti-CD3, APC-conjugated	BD Biosciences	Cat# 553066; RRID: AB_398529
Rat monoclonal anti-CD4, PE-Cy7-conjugated	eBioscience	Cat# 25–0042-82; RRID: AB_469578
Rat monoclonal anti-CD45, FITC-conjugated	BD Biosciences	Cat# 553080; RRID: AB_394610
Rat monoclonal anti-CD8, PE-conjugated	BD Biosciences	Cat# 553033; RRID: AB_394571
Rat monoclonal anti-F4/80, PerCP-conjugated	eBioscience	Cat# 45–4801; RRID: AB_914344
Bacterial and Virus Strains		
AAV-DJ-EF1a-DIO-TATAlox-DSE-EYFP-shiNOS-2	This paper	N/A
AAV-CMV-GFP	Vector Biolabs	Cat# 7101
AAV-Cre-GFP	SignaGen	Cat# SL100814
Chemicals, Peptides, and Recombinant Proteins		
Zoletil®	Virbac	Cat# 5G45
Rompun®	Bayer	Cat# 2138S
BODIPY-493/503	Invitrogen	Cat# D3922; CAS: 121207–31-6
Bromouridine	Sigma	Cat# B5002; CAS: RN 59–14-3
Alexa-fluoro 680-conjugated albumin	Molecular Probes	Cat# A34787
BODIPY-labeled fluorescent fatty acid	Invitrogen	Cat# D3835; CAS: 158757–84-7
Insulin (Humulin-R®)	Eli Lilly	Cat# HI0210
Leptin	R&D Systems	Cat# 498-OB
Angiotensin-2	Sigma	Cat# A9525; CAS: 4474–91-3
Fluoresbrite®	Polysciences	Cat# 17155–2
N^G-Nitro-D-arginine methyl ester hydrochloride (D-NAME)	Sigma	Cat# N4770; CAS: 50912–92-0
N^G-Nitro-L-arginine methyl ester hydrochloride (L-NAME)	Sigma	Cat# N5751; CAS: 51298–62-5

REAGENT or RESOURCE	SOURCE	IDENTIFIER
L-N^6-(1-Iminoethyl)lysine dihydrochloride (L-NIL)	Cayman Chemical	Cat# 80310; CAS: 159190–45-1
Sodium nitroprusside	Sigma	Cat# 1614501; CAS:13755–38-9
Critical Commercial Assays		
Nitrate/nitrite colorimetric assay kit	Cayman Chemical	Cat# 780001
Insulin ELISA kit	ALPCO	Cat# 80-INSMSU-E01
Triglyceride colorimetric assay kit	Cayman Chemical	Cat# 10010303
TNFα ELISA kit	R&D Systems	Cat# MTA00B
Experimental Models: Cell Lines		
Mouse: BV2 microglial cell-line	Obtained from Dr. Rina Yu (University of Ulsan, Korea)	N/A
Mouse: RAW264.7 monocyte/macrophages cell-line	ATCC	Cat# TIB-71
Experimental Models: Organisms/Strains		
Mouse: C57BL/6	Orient Bio	N/A
Mouse: LysM-*cre*: B6.129P2-Lyz2$^{tm1(cre)Ifo}$/J	Jackson Laboratory	Cat# JAX: 004781
Mouse: GFP-*loxP*: B6.129(Cg)-Gt(ROSA)26Sor$^{tm4(ACTB-tdTomato,-EGFP)Luo}$/J	Jackson Laboratory	Cat# JAX: 007676
Mouse: tdTomato-loxP: B6.Cg-Gt(ROSA)26Sor$^{tm9(CAG-tdTomato)Hze}$/J	Jackson Laboratory	Cat# JAX: 007909
Oligonucleotides		
Primers for *Angiopoietin-1*, see Table S1	This paper	N/A
Primers for *Angiopoietin-2*, see Table S1	This paper	N/A
Primers for *Gapdh*, see Table S1	This paper	N/A
Primers for *Hif-1α*, see Table S1	This paper	N/A
Primers for *Il-1β*, see Table S1	This paper	N/A
Primers for *Il-6*, see Table S1	This paper	N/A
Primers for *Nos2* (*iNos*), see Table S1	This paper	N/A
Primers for *Nos3* (*eNos*), see Table S1	This paper	N/A
Primers for *Ptp1b*, see Table S1	This paper	N/A
Primers for *Socs3*, see Table S1	This paper	N/A
Primers for *Tnfa*, see Table S1	This paper	N/A
Primers for *Vegfa*, see Table S1	This paper	N/A
Primers for *Vegfr2*, see Table S1	This paper	N/A
Recombinant DNA		
Mouse *Nos2* (*iNos*) shRNA; 5′-TAGCACAGAATGTTCCAGAATC TTCAAGAGAGATTCTGGAACATTCTGTGCTTTTTTTG-3	This paper	N/A
Software and Algorithms		
ImageJ	NIH	https://imagej.nih.gov/ij/
SPSS (version 24)	IBM	N/A
Photoshop CS6	Adobe	https://www.adobe.com
Prism 5	GraphPad	https://www.graphpad.com/scientific-software/prism/
Other		
Stainless steel internal cannula	Plastics One	Cat# C315i/Spc

REAGENT or RESOURCE	SOURCE	IDENTIFIER
Stainless steel guide cannula	Plastics One	Cat# C315G/Spc
Stainless steel dummy cannula	Plastics One	Cat# C315DC
ALZET osmotic pump	Alzet	Cat# 1004
Accu-Chek glucometer	Roche Diabetes Care	Cat# GC04640323
Standard Chow diet	Cargill Agri Purina	Cat# 38057
High fat diet	Research Diets	Cat# D12492

CONTACT FOR REAGENT AND RESOURCE SHARING

Further information and requests for reagents may be directed to and will be fulfilled by the Lead Contact, Min-Seon Kim (mskim@amc.seoul.kr).

EXPERIMENTAL MODEL AND SUBJECT DETAILS

Animals—All animal procedures were approved by the Institutional Animal Care and Use Committee of the Asan Institute for Life Science (Seoul, Korea) and the Korean Advanced Institute of Science and Technology (Daejeon, Korea). Seven weeks-old C57BL/6 male mice were purchased from Orient Bio (Seongnam, Korea). Lysozyme M (LysM)-*cre* mice (The Jackson Laboratory) on the C57BL/6 genetic background were mated with mice that had an enhanced green fluorescent protein (GFP) or a tdTomato (tdT) reporter allele with an upstream *loxP*-flanked STOP cassette (both from The Jackson Laboratory) to generate LysM^{GFP} and LysM^{tdT} mice. Only male mice were used in our study as female mice were resistant to develop HFD-induced hypothalamic inflammation and obesity. Animals were housed under controlled temperature ($22 \pm 1°C$) and a 12 h light-dark cycle (lights on 8 AM). Mice had free access to a standard chow diet (12.5% of calorie from fat; Cargill Agri Purina) and water unless indicated otherwise. To generate diet-induced obesity, mice were fed a high fat diet (fat 58%, Research Diets) from 7 weeks of age for indicated period.

Cell lines—RAW264.7 macrophages (ATCC, passage # 8) and BV2 microglial cells (from Rina Yu at the University of Ulsan, passage # 9) were maintained in DMEM supplemented with 10% fetal bovine serum and 1% penicillin/streptomycin and subcultured every 2 days.

METHOD DETAILS

Immunostaining—Mice were anesthetized with intraperitoneal injection of 40 mg/kg Zoletil®and 5 mg/kg Rompun®, and then perfused with 50 mL saline followed by 50 mL 4% paraformaldehyde (PFA) via the left ventricle of heart. Whole brains were collected, fixed with 4% PFA for 24 h, and dehydrated in 30% sucrose solution until brains sank to the bottom of the container. Coronal brains including the hypothalamus were sectioned 30 μm thick using a cryostat (Leica, Wetzlar, Germany). One of every five slices (about 10 brain slices per each animal) was collected. Sections were stored at 70°C. LysM^{GFP} cells, microglia, astrocytes, neurons, and blood vessels were immunostained as follows. Hypothalamic slices were permeabilized in 0.5% PBST for 5 min, blocked with 5% normal donkey serum (at room temperature [RT] for 1 h) and incubated with primary antibodies for GFP (1:1000), Iba1 (1:500), GFAP (1:200), MAP2 (1:500), or PECAM1 (1:200) at 4°C for 16 h and then at RT for 1 h. For CD169 and Ki67 double staining, hypothalamic slices were

blocked with 5% BSA and incubated with anti-Ki67 antibody (1:100) and anti-CD169 antibody (1:100) at 4°C for 16 h and then at RT for 1 h. For iNOS staining, slices were blocked with 5% goat normal serum and then incubated with anti-iNOS antibody (1:100) at 4°C for 16 h and then at RT for 1 h. After washing, slides were incubated with the appropriate Alexa-Flour 488-, 633-, or 647-conjugated secondary antibodies (1:1000) at RT for 1 h. For BrdU staining, brain slices were incubated with 2 N HCl for 30 min, permeabilized in 0.1% PBST for 5 min, and blocked with 3% goat serum for 1 h. Afterward, they were incubated with anti-BrdU antibody (1:400) at 4°C for 16 h, and then at RT for 1 h.

For P-STAT3 staining, whole brains were collected without perfusion, snap frozen, and stored at –70°C. Brains were sectioned using a cryostat. Fresh-frozen hypothalamic slices were fixed in 4% PFA for 30 min, blocked with 5% normal donkey serum, and incubated with P-STAT3 primary antibody (1:1000) at 4°C for 16 h and then at RT for 1 h. For nuclear staining, slides were treated with DAPI (1:10000) for 10 min before mounting. Immunofluorescence was imaged using a confocal microscopy (Carl Zeiss 780, Germany). Fluorescence quantitation and cell counting was performed throughout the entire rostro-caudal axis of the ARC (about 10 brain sections per animal). Fluorescence intensity was measured using ImageJ.

Intracerebroventricular injection of chemicals—A stainless steel cannula (26 gauge) was implanted into the lateral ventricle (LV) of C57BL/6 or LysM^GFP mice (stereotaxic coordinates: 0.6 mm caudal to bregma, 1 mm right to the sagittal sinus, and 2.0 mm ventral to the sagittal sinus). Following a 7-day recovery period, the correct positioning of each cannula was confirmed by observing a positive following administration of 50 ng angio-tensin-2. Animals with a negative drinking response to angiotensin-2 were excluded for further studies. Sodium nitroprusside (1 μg), L-NAME (0.1 μg), D-NAME (0.1 μg), and L-NIL (0.1 μg) were purchased from Sigma, dissolved in 2 μL saline and administered daily via the LV-implanted cannula during the early light phase for 5 days. Body weight and food intake were monitored daily. On the 6th day, one half of treated or untreated mice was perfused with 4% PFA, and whole brains were collected for GFP immunostaining. The other half of mice treated with sodium nitroprusside, L-NIL or D-NIL was sacrificed, and mediobasal hypothalamic blocks were collected to determine the hypothalamic inflammatory cytokine mRNA expression using qPCR. The experiments were repeated at least twice.

Bromodeoxyuridine study—5-bromodeoxyuridine (BrdU) was diluted in normal saline and injected into the peritoneal cavity once a day for 5 days (100 mg/kg/day). On the 5th day of injection, mice were cardiac-perfused with 4% PFA 1 h after BrdU injection. Whole brain was collected and cut into 30 μm-thick slices. Brain slices were subjected to BrdU immunostaining.

Hypothalamic gene expression—CD- or 20-week HFD-fed mice were kept under freely-feeding conditions and sacrificed by decapitation in the early light phase. Mediobasal hypothalamic tissue blocks were collected, snap frozen in liquid nitrogen, and stored at –70°C. Total RNA was extracted using TRIzol (Life Technologies) according to the manufacturer's protocol. RNA (5 mg) was reverse transcribed to generate cDNA. The

mRNA expression level was determined using real-time PCR analysis using the primers (Table S1). The mRNA expression levels were normalized to that of glyceraldehyde 3-phosphate dehydrogenase (GAPDH).

LysM+ cell-specific iNOS knockdown—Small hairpin RNA (shRNA) targeting murine NOS2, which encodes iNOS, was cloned into the pAAV-EF1a-DIO-TATAlox-EYFP-U6 vector in which iNOS shRNA was designed to be expressed in a Cre-dependent manner (Figure 4A). Before generating AAV, successful iNOS knockdown was tested in RAW264.7 cells by cotransfecting pAAV-EF1a-DIO-TATAlox-DSE-EYFP-shiNOS and Cre-recombinase AAV. Cells were harvested 72 h after transfection and following 24 h-palmitate treatment (500 μM) (Figure 4B). iNOS expression was determined by western blotting using anti-iNOS antibody (BD Biosciences, #610328). AAV-DJ-EF1a-DIO-TATAlox-DSE-EYFP-shiNOS-AAV was produced by Vector Biolabs (Malvem, PA). The shiNOS-AAV (3.4 3 10^9 genome copies in 400 nl) was microinjected bilaterally into the ARC (6.1 mm deep, 1.6 mm caudal to bregma, 0.1 mm lateral from the sagittal suture) of LysM^{tdT} or LysM^{GFP} mice under anesthesia via a syringe pump (Harvard Apparatus, Holliston, MA) at a rate of 40 nl/min for 10 min (400 nl/injection site). Control animals were injected with the same amount of GFP-AAV (Vector Biolabs). Successful injection of AAV was verified by YFP expression or suppressed iNOS expression in ARC LysM+ cells (Figures 4C and 4D). Results from animals with successful injections were included in the data analyses. The experiments were repeated twice.

Leptin sensitivity test in NOS inhibitor-treated DIO mice—Leptin (1 μg) was dissolved in normal saline before injection and administered intracerebroventricularly in a 2 μL volume during the early light phase on the 5th day of L-NAME or L-NIL treatment. Food and body weight were monitored for 24 h post-leptin injection. Some mice were cardiac perfused at 45 min after ICV leptin injection for P-STAT3 immunohistochemistry. The experiments were repeated at least twice.

Osmotic pump study—ALZET osmotic pumps were implanted subcutaneously in the inter-scapular area in CD- or 20-week HFD-fed LysM^{GFP} mice and connected to an LV-implanted cannula via a polyvinyl catheter (Alzet; Brain infusion kit 1). L-NIL was infused into the LV at a rate of 1.2 ng/h for 4 weeks. During the treatment period, food intake and body weight were monitored weekly. Fat mass was measured using dual X-ray absorptiometry (Lunar PIXImus, London, UK) before sacrificed. Metabolic studies were performed during the 3rd and 4th treatment weeks. At the end of the study, mice were sacrificed to collect blood, epididymal fat tissue and brains following a 5 h fast. Some of animals underwent euglycemic clamp study just before sacrificed.

Glucose, insulin, and pyruvate tolerance tests—For glucose tolerance test, D-glucose (1 g/kg, Sigma) was administrated via oral route in overnight fasted-mice, For insulin and pyruvate tolerance test, insulin (Humulin-R® 0.25 U/kg, Eli Lilly) or pyruvate (2 g/kg, Sigma) were injected into the peritoneum in overnight fasted-mice. Blood samples were obtained from a tail vein for glucose measurement immediately before and 15, 30, 60,

90, and 120 min after injections. Glucose levels were measured using a glucometer (ACCU-CHEK®, Aviva Plus System).

Plasma glucose, insulin, triglyceride, and TNFα—Plasma was collected following an overnight fast. Glucose concentrations were measured using a glucometer. Plasma insulin and TNFα concentrations were assayed using commercial ELISA kits. Triglyceride levels were measured using a colorimetric assay kit (Cayman Chemical). Homeostatic model assessment for insulin resistance (HOMA-IR) was calculated using the following formula: [fasting glucose (mM/l) x fasting insulin (IU/ml)]/22.5.

Pancreatic basal insulin-euglycemic clamp—Pancreatic basal insulin clamp was performed as previously described (Mighiu et al., 2013). A venous catheter was surgically implanted in the right jugular vein of DIO mice with or without L-NIL treatment for 4 weeks under anesthesia using Zoletil®/Rompun®. Pancreatic clamp was performed after 3–4 days of recovery. The mice were fasted overnight before clamp and placed in a plastic restrainer from t = 90 min to t = 0 min for adaptation. At t = 0 min, a primed-continuous intravenous infusion of [3-^{3}H]-glucose (1 μCi bolus and then 0.1 μCi min^{-1}; Perkin Elmer) was initiated and maintained throughout the clamp period. A pancreatic euglycemic clamp began at t = 60 min and lasted until 150 min, during which SRIF (1.1 μg kg^{-1}min^{-1}) and insulin (0.8 mU kg^{-1}min^{-1}) were infused concurrently to suppress endogenous insulin and glucagon secretion and to maintain basal insulin concentrations, respectively. An infusion of 10% glucose solution was used to maintain plasma glucose concentrations to the level prior to insulin infusion. Blood samples were collected at 10 min intervals from the cut tail to measure blood glucose levels and [3-^{3}H]-glucose specific activity. Plasma concentrations of [3-^{3}H]-glucose were determined following deproteinization of plasma samples with 20 μl zinc sulfate and barium hydroxide. Glucose infusion rate (GIR) was measured throughout the clamp. Basal glucose turnover and insulin-stimulated glucose disappearance rate (Rd) were represented by the ratio of the [3-^{3}H]-glucose infusion rate to the specific activity of plasma glucose at the end of basal period and during clamp steady-state, respectively. Hepatic glucose production during the clamp was represented by subtracting steady-state GIR from Rd, and presented as % suppression of basal values during clamp period.

Measurement of nitric oxide—Brain tissues including the hypothalamus (50 mg) were minced in 400 μL PBS and centrifuged at 10,000 × *g* and 4°C for 10 min. Tissue supernatant (80 μl) and plasma (40 μl) were assayed using the nitrate/nitrite colorimetric assay (Cayman Chemical) to measure nitric oxide concentrations.

Adipose tissues immune cell analysis—Epididymal adipocyte tissue was minced and dissociated into single cells using 1 mg/ml collagenase D-containing RPMI media. Cells were incubated for 1 h at 37°C and centrifuged at 300 × *g* for 5 min. Pellets were collected and filtered through nylon mesh with 70 μm pores. To label leukocytes, macrophages, B cells, and T cells, the dissociated tissue cells were incubated with antibodies against CD45, F4/80, CD11b, B220, CD3, CD4, and CD8 (1:200 dilution) for 1 h. After washing with PBS, cells processed using flow cytometry (BD FACS Canto; BD Biosciences).

Phagocytosis assay—To test the effect of L-NIL on the phagocytic activity of microglia and macrophages *in vitro*, BV2 microglial cells and RAW264.7 macrophage cells were treated with L-NIL (50 μM) or palmitate (500 μM) at 37°C for 6 h. During the last 30 min-treatment period, cells were reacted with Fluoresbrite® yellow green microsphere 3.0 μm particles (10^8 particles per 1 mL medium). Cells were washed twice with PBS and collected for FACS analysis. In the in vivo experiment, C57 mice were injected with L-NIL (0.1 μg) or saline via lateral ventricle (LV)-implanted cannulae for 5 days. Mice were sacrificed 1 h after the last L-NIL injection on the 5th day. Fluoresbrite® (2×10^7 particles in 2 μl) were injected via the LV cannulae 36 h before sacrifice. Whole brain was collected, sliced, and immunostained with $Iba1^+$ antibody. Fluoresbrite particles inside $Iba1^+$ microglia were examined using confocal microscopy.

Vascular permeability test—To test hypothalamic vascular permeability, Alexa-Fluoro 680-conjugated albumin (10 mg/kg diluted in saline) or BODIPY-labeled fluorescent fatty acid (10 mg/kg diluted in 20% DMSO) was administered via a tail vein. Whole brains were collected 20 min after injection, immediately frozen, and sliced. For Fluoro-albumin study, slices were immunostained for PECAM1. Immunofluorescence images were collected using a confocal microscope. All vascular permeability tests were performed during the early light period under free-feeding conditions.

QUANTIFICATION AND STATISTICAL ANALYSIS

All data are presented as the mean ± standard error of the mean (SEM). Statistical analyses were performed using SPSS version 24 (IBM Analytics, North Castle, NY). Cell numbers and immunofluorescence intensity were quantified using ImageJ (NIH) or Photoshop version CS6 (Adobe Systems, San Jose, CA). The sample sizes were selected based on previous studies with similar methodologies. Before studies, animals were randomized into subgroups based on their body weights so as to match the average body weight of each group. Animals in that AAV injections failed to target the ARC were excluded for the data analysis. Statistical significance among the groups was tested using one-way or repeated-measures analysis of variance (ANOVA) followed by a post hoc least significant difference (LSD) test or an unpaired Student's t test if appropriate. Statistical significance was defined as $p < 0.05$.

Supplementary Material

Refer to Web version on PubMed Central for supplementary material.

REFERENCES

Abbott NJ, Rönnbäck L, and Hansson E (2006). Astrocyte-endothelial interactions at the blood-brain barrier. Nat. Rev. Neurosci 7, 41–53. [PubMed: 16371949]

Ajami B, Bennett JL, Krieger C, Tetzlaff W, and Rossi FM (2007). Local self-renewal can sustain CNS microglia maintenance and function throughout adult life. Nat. Neurosci 10, 1538–1543. [PubMed: 18026097]

Amano SU, Cohen JL, Vangala P, Tencerova M, Nicoloro SM, Yawe JC, Shen Y, Czech MP, and Aouadi M (2014). Local proliferation of macrophages contributes to obesity-associated adipose tissue inflammation. Cell Metab. 19, 162–171. [PubMed: 24374218]

Arruda AP, Milanski M, Coope A, Torsoni AS, Ropelle E, Carvalho DP, Carvalheira JB, and Velloso LA (2011). Low-grade hypothalamic inflammation leads to defective thermogenesis, insulin resistance, and impaired insulin secretion. Endocrinology 152, 1314–1326. [PubMed: 21266511]

Buckman LB, Thompson MM, Moreno HN, and Ellacott KL (2013). Regional astrogliosis in the mouse hypothalamus in response to obesity. J. Comp. Neurol 521, 1322–1333. [PubMed: 23047490]

Buckman LB, Hasty AH, Flaherty DK, Buckman CT, Thompson MM, Matlock BK, Weller K, and Ellacott KL (2014). Obesity induced by a high-fat diet is associated with increased immune cell entry into the central nervous system. Brain Behav. Immun 35, 33–42. [PubMed: 23831150]

Cai D, and Liu T (2011). Hypothalamic inflammation: a double-edged sword to nutritional diseases. Ann. N Y Acad. Sci 1243, E1–E39. [PubMed: 22417140]

De Souza CT, Araujo EP, Bordin S, Ashimine R, Zollner RL, Boschero AC, Saad MJ, and Velloso LA (2005). Consumption of a fat-rich diet activates a proinflammatory response and induces insulin resistance in the hypothalamus. Endocrinology 146, 4192–4199. [PubMed: 16002529]

Gao Y, Ottaway N, Schriever SC, Legutko B, García-Cáceres C, de la Fuente E, Mergen C, Bour S, Thaler JP, Seeley RJ, et al. (2014). Hormones and diet, but not body weight, control hypothalamic microglial activity. Glia 62, 17–25. [PubMed: 24166765]

Ginhoux F, and Jung S (2014). Monocytes and macrophages: developmental pathways and tissue homeostasis. Nat. Rev. Immunol 14, 392–404. [PubMed: 24854589]

Ginhoux F, Greter M, Leboeuf M, Nandi S, See P, Gokhan S, Mehler MF, Conway SJ, Ng LG, Stanley ER, et al. (2010). Fate mapping analysis reveals that adult microglia derive from primitive macrophages. Science 330, 841–845. [PubMed: 20966214]

Glass CK, and Olefsky JM (2012). Inflammation and lipid signaling in the etiology of insulin resistance. Cell Metab. 15, 635–645. [PubMed: 22560216]

Goldmann T, Wieghofer P, Jordão MJ, Prutek F, Hagemeyer N, Frenzel K, Amann L, Staszewski O, Kierdorf K, Krueger M, et al. (2016). Origin, fate and dynamics of macrophages at central nervous system interfaces. Nat. Immunol 17, 797–805. [PubMed: 27135602]

Gordon S, and Taylor PR (2005). Monocyte and macrophage heterogeneity. Nat. Rev. Immunol 5, 953–964. [PubMed: 16322748]

Gosselin D, Link VM, Romanoski CE, Fonseca GJ, Eichenfield DZ, Spann NJ, Stender JD, Chun HB, Garner H, Geissmann F, and Glass CK (2014). Environment drives selection and function of enhancers controlling tissue-specific macrophage identities. Cell 159, 1327–1340. [PubMed: 25480297]

Gregor MF, and Hotamisligil GS (2011). Inflammatory mechanisms in obesity. Annu. Rev. Immunol 29, 415–445. [PubMed: 21219177]

Hickey WF, and Kimura H (1988). Perivascular microglial cells of the CNS are bone marrow-derived and present antigen in vivo. Science 239, 290–292. [PubMed: 3276004]

Horvath TL, Sarman B, García-Cáceres C, Enriori PJ, Sotonyi P, Shanabrough M, Borok E, Argente J, Chowen JA, Perez-Tilve D, et al. (2010). Synaptic input organization of the melanocortin system predicts diet-induced hypothalamic reactive gliosis and obesity. Proc. Natl. Acad. Sci. USA 107, 14875–14880. [PubMed: 20679202]

Jais A, Solas M, Backes H, Chaurasia B, Kleinridders A, Theurich S, Mauer J, Steculorum SM, Hampel B, Goldau J, et al. (2016). Myeloidcell-derived VEGF maintains brain glucose uptake and limits cognitive impairment in obesity. Cell 165, 882–895. [PubMed: 27133169]

Kälin S, Heppner FL, Bechmann I, Prinz M, Tschöp MH, and Yi CX (2015). Hypothalamic innate immune reaction in obesity. Nat. Rev. Endocrinol 11, 339–351. [PubMed: 25824676]

Katashima CK, Silva VRR, Lenhare L, Marin RM, and Carvalheira JBC (2017). iNOS promotes hypothalamic insulin resistance associated with deregulation of energy balance and obesity in rodents. Sci. Rep 7, 9265. [PubMed: 28835706]

Kim MS, Yan J, Wu W, Zhang G, Zhang Y, and Cai D (2015). Rapid link-age of innate immunological signals to adaptive immunity by the brain-fat axis. Nat. Immunol 16, 525–533. [PubMed: 25848866]

Kreutzer C, Peters S, Schulte DM, Fangmann D, Türk K, Wolff S, van Eimeren T, Ahrens M, Beckmann J, Schafmayer C, et al. (2017). Hypothalamic inflammation in human obesity is mediated by environmental and genetic factors. Diabetes 66, 2407–2415. [PubMed: 28576837]

Lumeng CN, and Saltiel AR (2011). Inflammatory links between obesity and metabolic disease. J. Clin. Invest 121, 2111–2117. [PubMed: 21633179]

Mighiu PI, Yue JT, Filippi BM, Abraham MA, Chari M, Lam CK, Yang CS, Christian NR, Charron MJ, and Lam TK (2013). Hypothalamic glucagon signaling inhibits hepatic glucose production. Nat. Med 19, 766–772. [PubMed: 23685839]

Mildner A, Schlevogt B, Kierdorf K, Böttcher C, Erny D, Kummer MP, Quinn M, Brück W, Bechmann I, Heneka MT, et al. (2011). Distinct and non-redundant roles of microglia and myeloid subsets in mouse models of Alzheimer's disease. J. Neurosci 31, 11159–11171. [PubMed: 21813677]

Orthgiess J, Gericke M, Immig K, Schulz A, Hirrlinger J, Bechmann I, and Eilers J (2016). Neurons exhibit Lyz2 promoter activity in vivo: implications for using LysM-Cre mice in myeloid cell research. Eur. J. Immunol 46, 1529–1532. [PubMed: 27062494]

Pedroso JA, Buonfiglio DC, Cardinali LI, Furigo IC, Ramos-Lobo AM, Tirapegui J, Elias CF, and Donato J, Jr. (2014). Inactivation of SOCS3 in leptin receptor-expressing cells protects mice from diet-induced insulin resistance but does not prevent obesity. Mol. Metab 3, 608–618. [PubMed: 25161884]

Perreault M, and Marette A (2001). Targeted disruption of inducible nitric oxide synthase protects against obesity-linked insulin resistance in muscle. Nat. Med 7, 1138–1143. [PubMed: 11590438]

Perry VH, Nicoll JA, and Holmes C (2010). Microglia in neurodegenerative disease. Nat. Rev. Neurol 6, 193–201. [PubMed: 20234358]

Picardi PK, Calegari VC, Prada PO, Moraes JC, Araújo E, Marcondes MC, Ueno M, Carvalheira JB, Velloso LA, and Saad MJ (2008). Reduction of hypothalamic protein tyrosine phosphatase improves insulin and leptin resistance in diet-induced obese rats. Endocrinology 149, 3870–3880. [PubMed: 18467448]

Prinz M, Priller J, Sisodia SS, and Ransohoff RM (2011). Heterogeneity of CNS myeloid cells and their roles in neurodegeneration. Nat. Neurosci 14, 1227–1235. [PubMed: 21952260]

Rubenstein AH (2005). Obesity: a modern epidemic. Trans. Am. Clin. Climatol. Assoc 116, 103–113. [PubMed: 16555609]

Santoro A, Campolo M, Liu C, Sesaki H, Meli R, Liu ZW, Kim JD, and Diano S (2017). DRP1 suppresses leptin and glucose sensing of POMC neurons. Cell Metab. 25, 647–660. [PubMed: 28190775]

Schulz C, Gomez Perdiguero E, Chorro L, Szabo-Rogers H, Cagnard N, Kierdorf K, Prinz M, Wu B, Jacobsen SE, Pollard JW, et al. (2012). A lineage of myeloid cells independent of Myb and hematopoietic stem cells. Science 336, 86–90. [PubMed: 22442384]

Schwartz MW, Woods SC, Porte D, Jr., Seeley RJ, and Baskin DG (2000). Central nervous system control of food intake. Nature 404, 661–671. [PubMed: 10766253]

Serrats J, Schiltz JC, García-Bueno B, van Rooijen N, Reyes TM, and Sawchenko PE (2010). Dual roles for perivascular macrophages in immune-to-brain signaling. Neuron 65, 94–106. [PubMed: 20152116]

Smith JA, Das A, Ray SK, and Banik NL (2012). Role of pro-inflammatory cytokines released from microglia in neurodegenerative diseases. Brain Res. Bull 87, 10–20. [PubMed: 22024597]

Thaler JP, Yi CX, Schur EA, Guyenet SJ, Hwang BH, Dietrich MO, Zhao X, Sarruf DA, Izgur V, Maravilla KR, et al. (2012). Obesity is associated with hypothalamic injury in rodents and humans. J. Clin. Invest 122, 153–162. [PubMed: 22201683]

Valdearcos M, Robblee MM, Benjamin DI, Nomura DK, Xu AW, and Koliwad SK (2014). Microglia dictate the impact of saturated fat consumption on hypothalamic inflammation and neuronal function. Cell Rep. 9, 2124–2138. [PubMed: 25497089]

Valdearcos M, Douglass JD, Robblee MM, Dorfman MD, Stifler DR, Bennett ML, Gerritse I, Fasnacht R, Barres BA, Thaler JP, et al. (2017). Microglial inflammatory signaling orchestrates the hypothalamic immune response to dietary excess and mediates obesity susceptibility. Cell Metab. 26, 185–197.e3. [PubMed: 28683286]

Williams K, Alvarez X, and Lackner AA (2001). Central nervous system perivascular cells are immunoregulatory cells that connect the CNS with the peripheral immune system. Glia 36, 156–164. [PubMed: 11596124]

Yi CX, Gericke M, Krüger M, Alkemade A, Kabra DG, Hanske S, Filosa J, Pfluger P, Bingham N, Woods SC, et al. (2012). High calorie diet triggers hypothalamic angiopathy. Mol. Metab 1, 95–100. [PubMed: 24024123]

Highlights

- Chronic exposure to HFD activates and accumulates macrophages in the hypothalamus

- HFD increases iNOS expression in the hypothalamic perivascular macrophages

- Macrophage iNOS triggers hypothalamic inflammation and vascular hyperpermeability

- Inhibition of hypothalamic macrophage iNOS improves glucose metabolism in obese mice
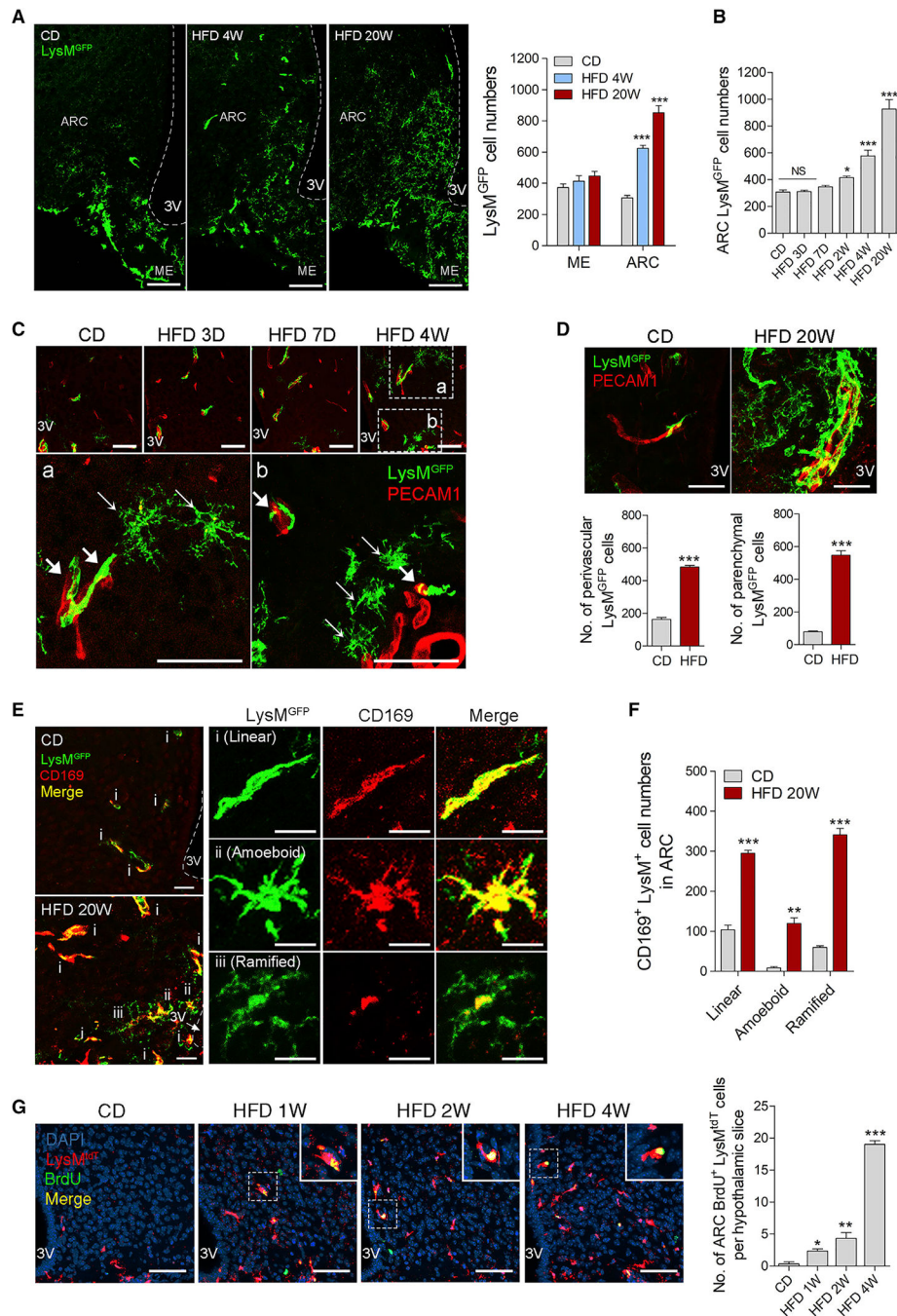
Figure 1. Expansion of Hypothalamic LysM^{GFP} Cells in Mice with Long-Term HFD Feeding

(A) Immunohistochemistry and quantification of LysM^{GFP} cells of the hypothalamic arcuate nucleus (ARC) and median eminence (ME) in LysM^{GFP} mice fed a standard chow diet (CD) or a high-fat diet (HFD) (58% fat) for 4 and 20 weeks. n = 5~7. Scale bars: 100 mm. 3V, third ventricle.

(B) Quantification of GFP$^+$ cells in the ARC of LysM^{GFP} mice fed CD or HFD for the indicated periods. n = 5~7.

(C) Double staining of GFP and platelet and endothelial cell adhesion molecule 1 (PECAM1) in the ARC of LysM[GFP] mice fed a CD or HFD for indicated time periods. Thin arrows: parenchymal LysM[GFP] cells. Thick arrows: perivascular LysM[GFP] cells. Scale bars: 100 μm.

(D) Quantification of perivascular and parenchymal GFP$^+$ cells in the ARC of LysM[GFP] mice fed CD and HFD for 20 weeks. n = 5~7. Scale bars: 25 μm.

(E and F) Double staining (E) and quantification (F) of GFP and macrophage marker CD169 in the ARC of LysM[GFP] mice fed CD or HFD for 20 weeks. (i) linear CD169^{high} LysM[GFP] cells, (ii) amoeboid CD169^{high} LysM[GFP] cells, and (iii) ramified microglia-like CD169^{low} LysM[GFP] cells are shown. n = 4~5. Scale bars: 25 μm.

(G) Confocal images and quantification of BrdU$^+$ LysM[tdT] cells in the ARC of LysM[tdT] mice on HFD for indicated periods. n = 3. Scale bars: 100 μm.

In (A), (B), (D), (F), and (G), data are presented as means ± SEM. *p < 0.05, **p < 0.01, and ***p < 0.005 versus CD. One-way ANOVA followed by a post hoc least significant difference (LSD) test was used for (A), (B), and (G). Unpaired Student's t test was used for (D) and (F). See also Figure S1.
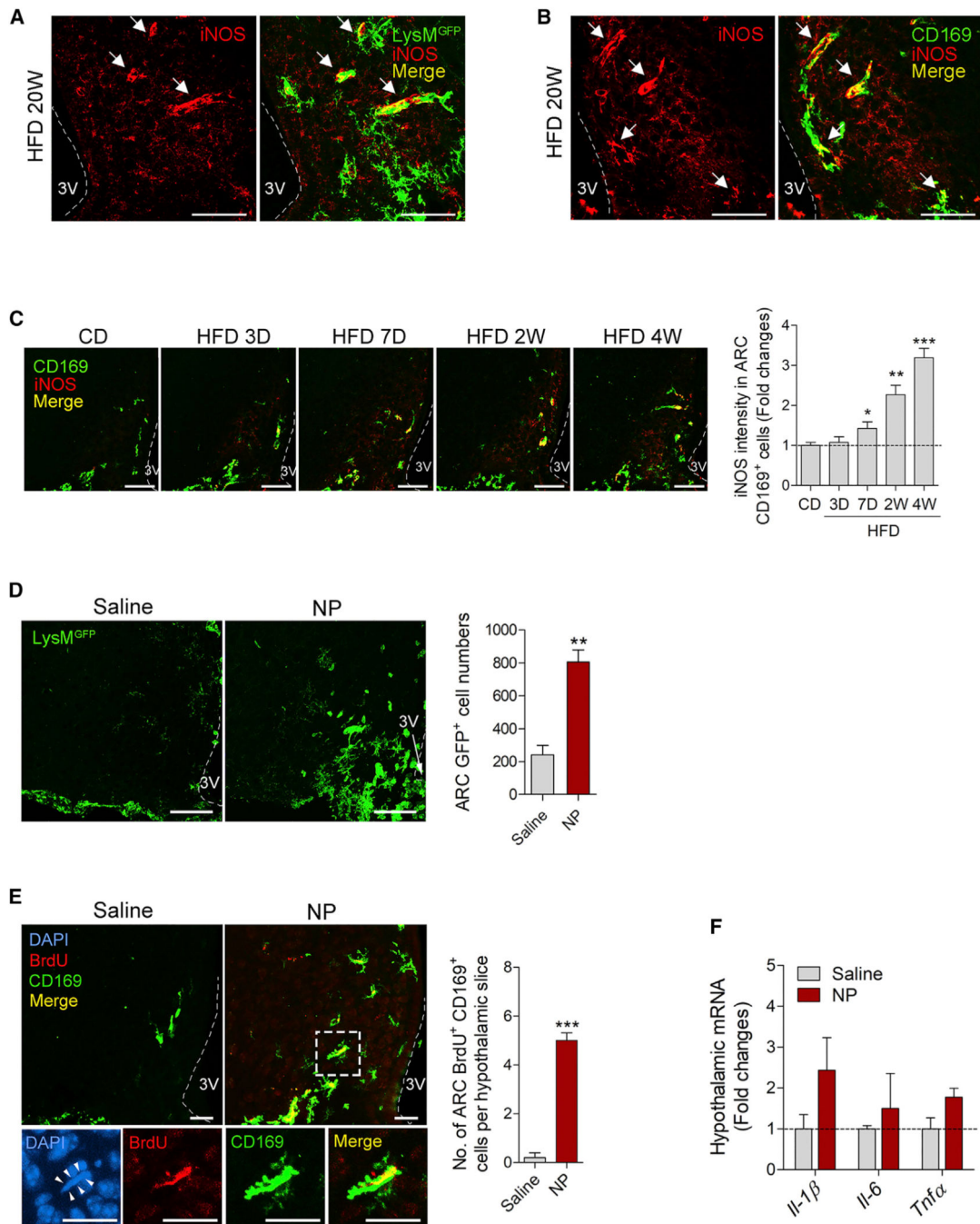
Figure 2. HFD Induces Enhanced iNOS Expression in ARC LysM+ CD169+ Macrophages
(A) Double staining of GFP and iNOS in the ARC of 20-week HFD-fed LysM^{GFP} mice. Arrows indicate linear LysM^{GFP} cells with strong iNOS expression. Scale bars: 100 μm.
(B) iNOS/CD169 double staining in the ARC of C57BL/6 mice fed HFD for 20 weeks. Arrows indicate strong iNOS immunoreactivity in linear CD169+ cells. Scale bars: 100 μm.
(C) Time course study showing iNOS expression in CD169+ ARC macrophages in mice fed HFD for indicated periods. n = 3. Scale bars: 100 μm.

(D) Confocal images and quantification of GFP$^+$ cells in the ARC of lean LysM^{GFP} mice injected saline or sodium nitroprusside (NP). Mice received a daily ICV injection of saline or 1 mg NP for 5 days. n = 3. Scale bars: 100 μm.

(E) BrdU and CD169 double staining and quantification in the ARC of C57BL/6 mice treated with ICV saline or NP. Arrows indicate BrdU$^+$ CD169$^+$ macrophages. n = 5. Scale bars: 100 μm.

(F) qPCR analysis of *Il-1β*, *Il-6*, and *Tnfa* mRNA expression in the MBH of mice receiving daily ICV injections of saline or NP for 5 days. n = 3.

In (C)–(F), data are presented as means ± SEM. *p < 0.05, **p < 0.01, and ***p < 0.005 versus CD or saline. One-way ANOVA followed by a post hoc LSD test was used for (C). Unpaired Student's t test was used for (D)–(F). See also Figure S2.
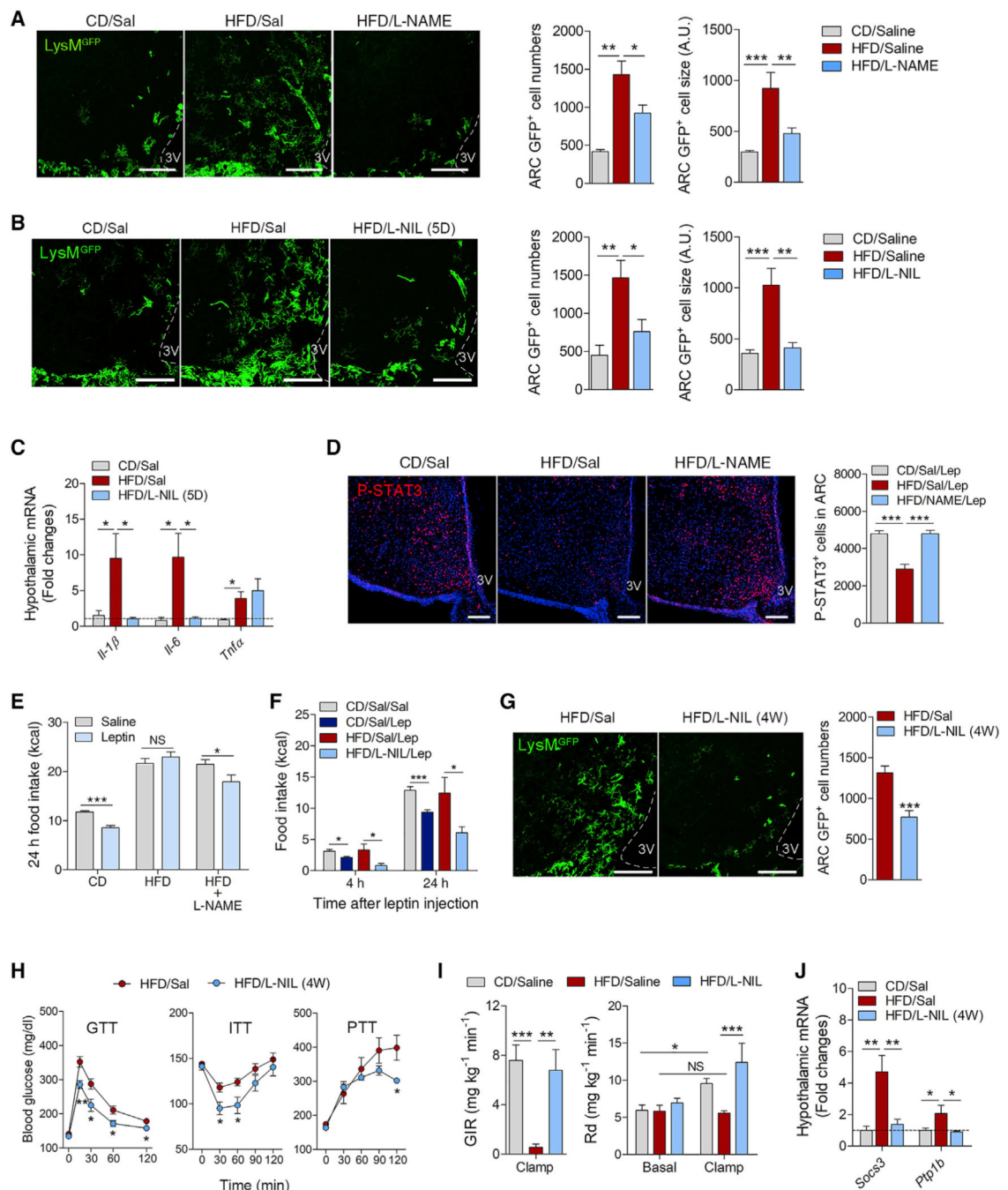
Figure 3. Hypothalamic iNOS Inhibition Ameliorates Hypothalamic Macrophage Expansion or Activation and Impaired Systemic Glucose Metabolism in DIO Mice

(A–C) Confocal images and quantification of GFP+ cells (A and B) and qPCR analysis of *Il-1β*, *Il-6*, and *Tnfα* (C) in the ARC of LysM[GFP] mice fed a CD or an HFD for 20 weeks and ICV injected daily with either saline, 0.1 mg L-NAME (A), or 0.1 mg L-NIL (B) for 5 days before sacrifice. n = 4~6. Scale bars: 100 μm. A.U., arbitrary unit.

(D–F) ICV leptin (1 μg)-induced anorexia and phosphorylated STAT3 (P-STAT3) expression (D) in mice fed CD or HFD for 20 weeks and treated with or without ICV L-NAME (E) or L-NIL (F) for 5 days. n = 4~5. Scale bars: 100 μm.

(G and J) Confocal images and quantification of GFP$^+$ cells (G) and qPCR analysis of *Socs3* and *Ptp1b* (J) in the ARC of 20-week HFD-fed LysM^{GFP} mice receiving ICV saline or L-NIL (1.2 ng/hr) for 4 weeks. n = 5~6. Scale bars: 100 μm.

(H) Glucose, insulin, and pyruvate tolerance tests (GTT, ITT, and PTT) in mice fed an HFD for 20 weeks and treated with ICV L-NIL for 4 weeks. n = 5~6.

(I) Glucose infusion rate (GIR) and glucose disappearance rate (Rd) in the euglycemic clamp study. Mice were fed CD or HFD for 20 weeks and ICV injected with saline or L-NIL for 4 weeks. n = 5~6.

In (A)–(J), data are presented as means ± SEM. *p < 0.05, **p < 0.01, and ***p < 0.005 versus saline-injected HFDgroup at each time point or between indicated groups. NS, not significant. One-way ANOVA followed by a post hoc LSD test was used for (A)–(D), (I) (GIR data), and (J). Two-way ANOVA followed by a post hoc LSD test was used for (E) and (I) (Rd data). Repeated ANOVA followed by a post hoc LSD test was used for (H). Unpaired Student's t test was used for (G). See also Figures S3 and S4.
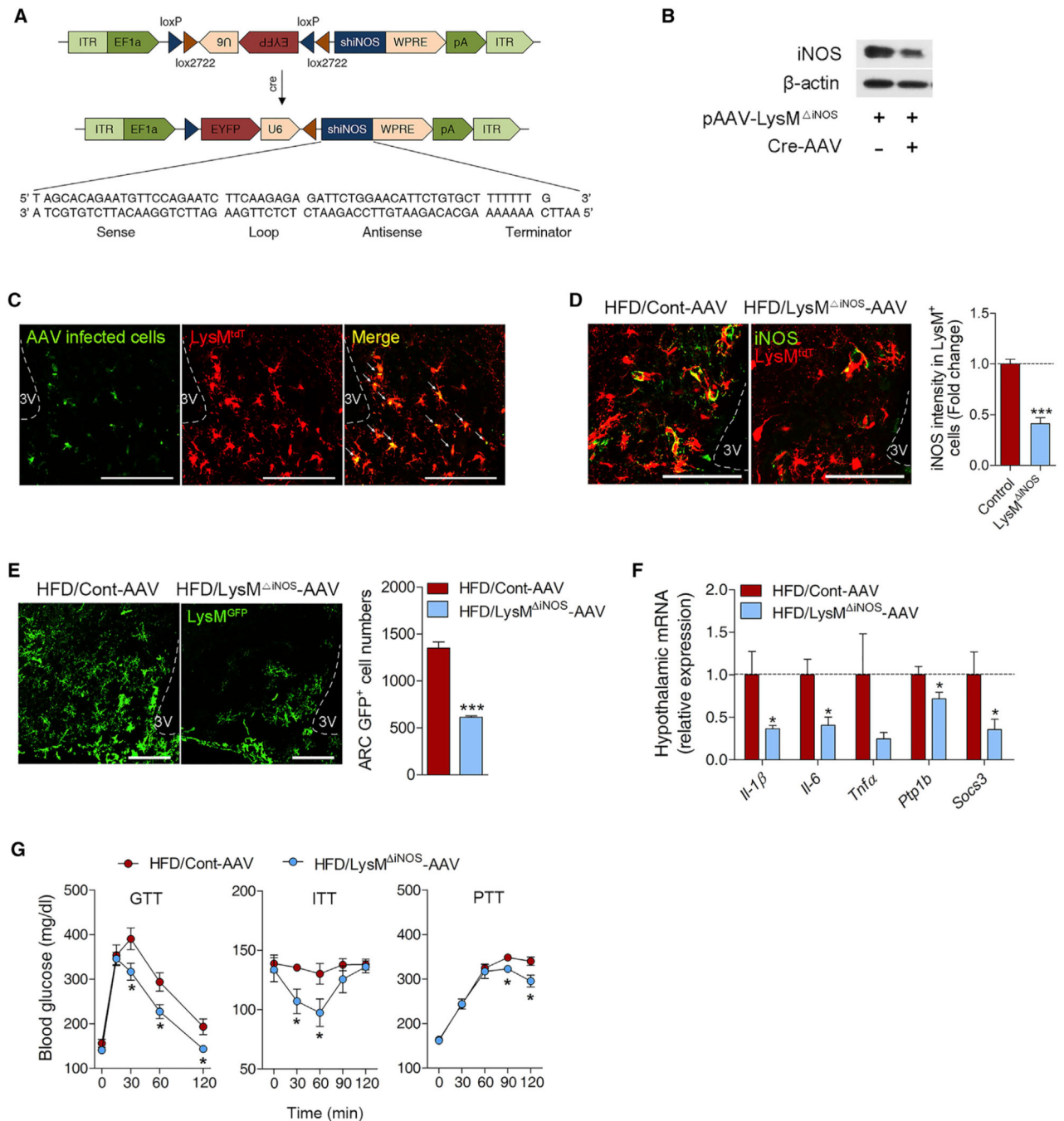
Figure 4. Macrophage iNOS Inhibition Mitigates HFD-Induced Hypothalamic Macrophage Activation and Glucose Dysregulation

(A) Construction of pAAV-YFP-LysM [iNOS].

(B) Immunoblotting showing *iNos* knockdown in RAW264.7 macrophage cells transfected with pAAV-YFP-LysM [iNOS] and Cre-recombinase-AAV.

(C) YFP and tdT double staining in the ARC of LysM[tdT] mice injected with YFP-LysM [iNOS]-AAV. Arrows indicate YFP[+] LysM[tdT] cells, demonstrating successful AAV transfection in the ARC LysM^{+} cells. Scale bars: 100 μm.

(D) Confocal images and quantification of iNOS and tdT double immunostaining in the ARC of LysM^{tdT} mice with intra-ARC injection of control-AAV or LysM ^{iNOS}-AAV. n = 3. Scale bars: 50 μm.

(E) Confocal images and quantification of GFP$^+$ cells in the ARC of LysM^{GFP} mice injected with control-AAV or LysM ^{iNOS}-AAV. n = 3. Scale bars: 100 μm.

(F and G) qPCR analysis of *Il-1β*, *Il-6*, *Tnfa*, *Socs3*, and *Ptp 1b* in the MBH (F) and GTT, ITT, and PTT (G) in DIO mice injected with control-AAV or LysM^{DiNOS}-AAV. n=5~6. In (D)–(G), data are presented as means ± SEM. *$p < 0.05$ and ***$p < 0.005$ versus Cont-AAV-injected HFD group. Unpaired Student's t test was used for (D)–(F). Repeated ANOVA followed by a post hoc LSD test was used for (G). See also Figure S5.
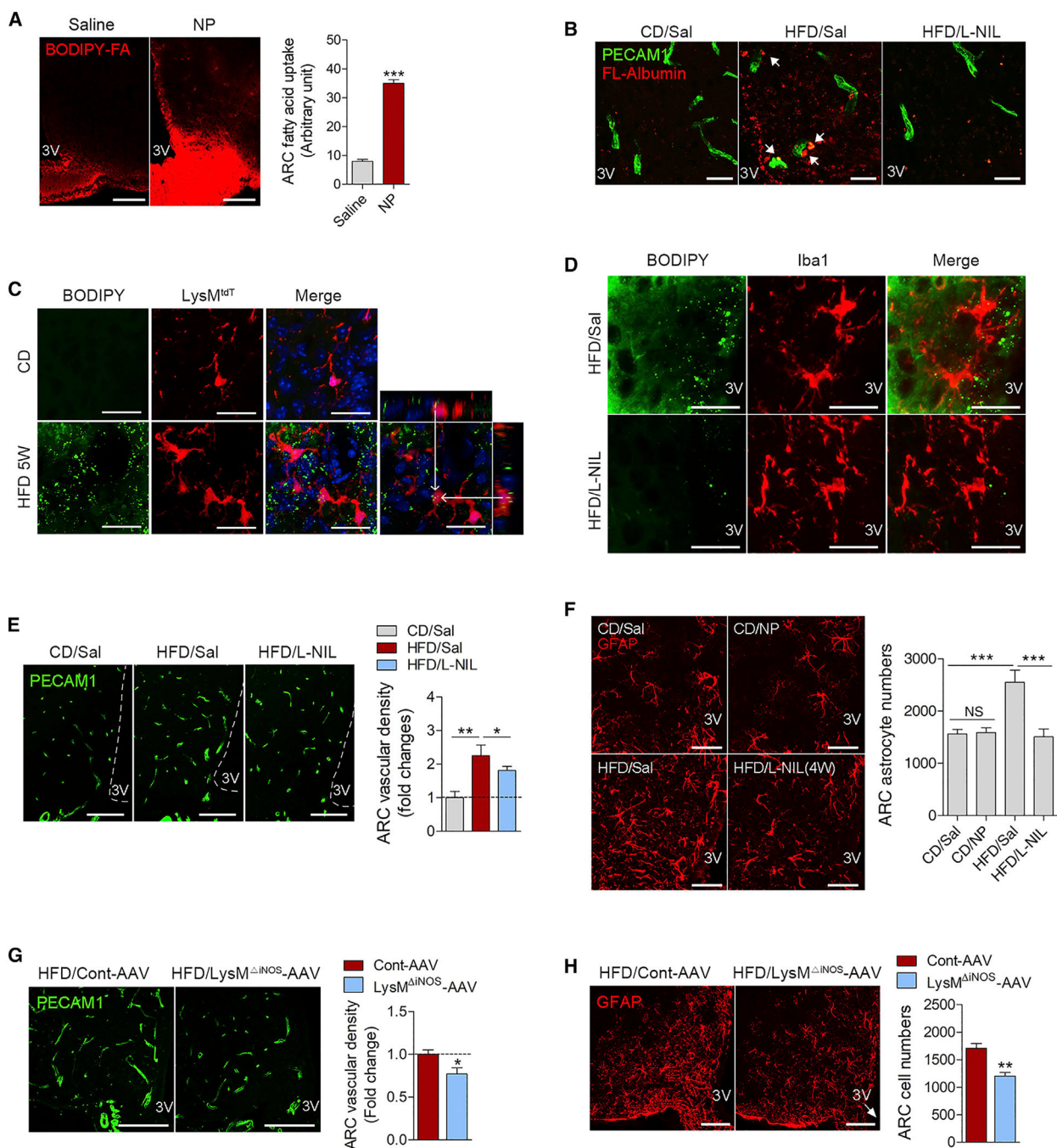
Figure 5. Hypothalamic iNOS Mediates HFD-Induced BBB Permeability, Astrogliosis, Lipid Flux, and Accumulation in the Hypothalamus

(A) Hypothalamic uptake of BODIPY-conjugated fatty acid in mice ICV injected daily with saline or 1 μg NP for 5 days. n = 6. Scale bars: 50 μm.

(B) Fluorescence images of fluorescence (FL)-conjugated albumin in the ARC of HFD-fed mice receiving saline or L-NIL (1.2 ng/hr for 4 weeks). Arrows indicate-extravasated albumin. Scale bars: 50 μm.

(C) Fluorescence images of BODIPY 493/503 in LysM^{tdT} mice fed an HFD for 5 weeks. Arrows indicate intracellular lipid droplets in LysM^{tdT} cells. Scale bars: 25 μm.

(D) Double fluorescence images of BODIPY 493/503 and Iba1 in the ARC of mice fed a CD or an HFD for 20 weeks either with or without ICV L-NIL infusion for4 weeks. Scale bars: 25 μm.

(E) Fluorescence images of PECAM1 staining in the ARC of mice fed a CD or an HFD for 20 weeks, either with or without 4-week ICV L-NIL infusion. n = 5~6. Scale bars: 100 μm.

(F) Confocal images of astrocyte marker glial fibrillary acidic protein (GFAP) in lean mice fed a CD, either with or without daily ICV NP treatments for 5 days, and in obese mice fed an HFD for 20 weeks, either with or without 4-week L-NIL treatment. n = 4~5. Scale bars: 50 μm.

(G and H) PECAM1 (G) and GFAP (H) immunostaining in the ARC of DIO mice with intra-ARC injection of control-AAV or LysM ^{iNOS}-AAV. n = 4~5. Scale bars: 100 μm.

In (A) and (E)–(H), data are presented as means ± SEM. *$p < 0.05$, **$p < 0.01$, and ***$p < 0.005$ versus control or between indicated groups. Unpaired Student's t test was used for (A), (G), and (H). One-way ANOVA followed by a post hoc LSD test was used for (E) and (F).